

The effect of temperature, interaction range, and pair potential on the formation of dodecagonal quasicrystals in core-corona systems

Harini Pattabhiraman and Marjolein Dijkstra

Soft Condensed Matter, Debye Institute for Nanomaterials Science, Department of Physics, Utrecht University, Princetonplein 5, 3584 CC, Utrecht, The Netherlands

E-mail: h.pattabhiraman@uu.nl and m.dijkstra@uu.nl

Received 31 October 2016, revised 12 December 2016

Accepted for publication 21 December 2016

Published 23 January 2017



Abstract

A two-dimensional dodecagonal quasicrystal was previously reported by Dotera *et al* (2014 *Nature* **506** 208) in a system of particles interacting with a hard core of diameter σ and a repulsive square shoulder of diameter $\delta = 1.40\sigma$. In the current work, we examine the formation of this quasicrystal using bond orientational order parameters, correlation functions and tiling distributions. We find that this dodecagonal quasicrystal forms from a fluid phase. We further study the effect of the width of the repulsive shoulder by simulating the system over a range of values of δ . For the range of densities and temperatures considered, we observe the formation of the dodecagonal quasicrystal between $\delta = 1.30\sigma$ and 1.44σ . We also study the effect of shape of the interaction potential by simulating the system using three other interaction potentials with two length scales, namely hard-core plus a linear ramp, modified exponential, or Buckingham (exp-6) potential. We observe the presence of the quasicrystal in all three systems. However, depending on the shape of the potential, the formation of the quasicrystal takes place at lower temperatures (or higher interaction strengths). Using free-energy calculations, we demonstrate that the quasicrystal is thermodynamically stable in the square-shoulder and linear-ramp system.

Keywords: dodecagonal quasicrystal, free energy, phase diagram

(Some figures may appear in colour only in the online journal)

1. Introduction

Quasicrystals are materials that exhibit long-range orientational order but no translational periodicity. They were first reported by Shechtman *et al* in a rapidly cooled Al–Mn alloy [1]. Since then, the world of quasicrystals has been blooming. Although, quasicrystals were initially found mostly in intermetallic systems, they have now also been reported in several soft-matter systems ranging from spherical dendrite micelles [2, 3], block copolymers [4–7] to binary mixtures of nanoparticles [8, 9]. Furthermore, there have been reports of colloidal quasicrystals obtained using external fields such as holography [10] or laser beams [11].

One of the most fascinating properties of quasicrystals is the formation of photonic band gaps which is relevant for applications in optical devices. Photonic quasicrystals were first described for a one-dimensional quasicrystal by Kohmoto *et al* and have been extensively studied since then in two- and three-dimensional systems [12–14]. In general, soft-matter photonic quasicrystals have potential interesting applications in the telecommunications sector which require materials with a photonic band gap in the visible region of light [15]. This is due to the larger size of the constituent particles than their atomic counterparts and the relative ease of formation by self-assembly [16, 17]. Correspondingly, a complete photonic bandgap was observed in a 12-fold symmetric quasicrystal

obtained by etching air holes through a planar wave guide [18]. However, to the best of our knowledge, a quasicrystal self-assembled from colloidal particles with a full photonic bandgap has not yet been realized experimentally. Thus, in order to facilitate the synthesis and self-assembly of these two-dimensional soft-matter quasicrystals, we investigate here extensively their formation and stability by computer simulations.

It is now widely accepted that the formation of quasicrystals in soft-matter systems is aided by the presence of two competing length scales [19–24]. This could either be the size of the two particle species in binary systems or an effective pair interaction that favours two length scales in a one-component system. Evidences have been found for both these classes using computer simulations. The former has been observed in particles interacting with Lennard–Jones [25, 26] and square-well [27] potentials, and the latter in systems with Lennard–Jones–Gauss [28], square-shoulder [29], square-well [30], linear ramp [31], flat-well [32] and three-well oscillating [33] pair interactions.

Computational studies of soft-matter quasicrystals using systems with core-corona architecture gained attention by the work of Dotera *et al* in which they studied the formation of quasicrystals of various symmetries using Monte Carlo simulations [29]. They reported six quasicrystals at different sizes of the corona with respect to the hard core. More recently, Schoberth *et al* studied the formation of quasicrystals using a more realistic model for core-shell micelles [34]. They used a repulsive-shoulder potential to account for the entropic interactions of the overlapping polymer brushes. They provide a comparison with the system used by Dotera *et al*. The focus of these two works has been to identify the regions of quasicrystal formation in density-corona diameter parameter space. One of the more appealing quasicrystals reported in both these studies is the high-density dodecagonal quasicrystal, which is more commonly observed in experimental soft-matter systems. Though there has been studies reported on the formation of a low-density dodecagonal quasicrystal [23, 24], we did not find any reports regarding the nature of formation of the high-density dodecagonal quasicrystal. Our present work is a step in this direction.

In this work, we study various aspects of the formation of a dodecagonal quasicrystal reported by Dotera *et al* in a system of particles interacting with a hard core and a square-shoulder potential with a shoulder range equal to 1.4 times the hard-core diameter [29]. We divide this study into three parts. In the first part, we qualitatively and quantitatively follow the formation of a dodecagonal quasicrystal in a core-corona system using bond orientational order parameters, correlation functions and tiling distributions. In the second and third parts, we analyse the robustness of the formation of the quasicrystal by respectively studying the effect of shoulder width and the shape of the interaction potential. The paper is organised as follows. We describe the details concerning our model, simulations and analysis methods in section 2. We present and discuss the results in section 3, and we end with conclusions in section 4.

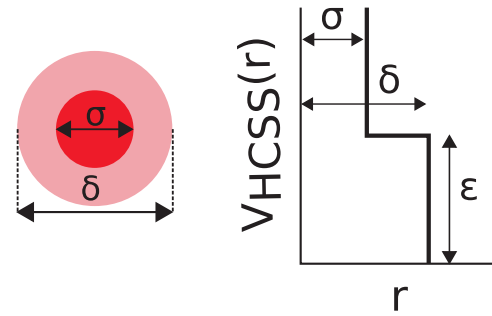


Figure 1. Schematic representation of the hard-core square shoulder (HCSS) potential, $V_{\text{HCSS}}(r)$, as a function of the interparticle distance r . σ and δ are, respectively, the diameter of the hard core and the square shoulder of the particle.

2. Methods

2.1. Model and simulations

In the first two parts of this study, we use a hard-core square shoulder (HCSS) model to represent the core-corona architecture. This model consists of a two-dimensional system of particles interacting with a pair potential consisting of a hard core of diameter σ and a repulsive square shoulder of diameter δ . This hard-core square shoulder (HCSS) pair potential, which was earlier used to model interparticle interactions in Cesium and Cerium [35], reads

$$V_{\text{HCSS}}(r) = \begin{cases} \infty, & r \leq \sigma \\ \epsilon, & \sigma < r \leq \delta, \\ 0, & r > \delta \end{cases} \quad (1)$$

where r is the distance between the centre-of-masses of two particles, and $\epsilon > 0$ is the shoulder height. We show a schematic representation of this pair potential in figure 1, where we represent the hard core and square shoulder by the dark and light circles. This step potential introduces two characteristic length scales in the system, respectively, at the hard core diameter σ and the square shoulder diameter δ . We consider the shoulder width in units of the hard core diameter. This ultimately results in a single tunable parameter in the system, i.e. the shoulder width δ .

The basis of this study is a dodecagonal quasicrystal at $\delta = 1.40\sigma$ initially reported in a simulation study by Dotera *et al* [29] and recently re-established by Schoberth *et al* [34]. In both works, bond orientational order parameters and bond orientation correlation functions were used to identify and characterise the resultant phase. However, the characterisation during the formation of this quasicrystal and details on its thermodynamic stability are absent. We had previously studied the thermodynamic stability of this dodecagonal quasicrystal with emphasis on its relative stability over approximants with various periodic square-triangle tilings [36]. We found that the quasicrystal is thermodynamically stable with respect to the considered tilings over the range of temperatures and densities that were studied. Therefore, we only consider this quasicrystal in the present work. Here, we critically evaluate the formation of this quasicrystal in terms of a number of order

parameters. This also acts as a summary of various methods that can be utilised to identify the quasicrystal. Further, we analyse the scope for formation of this quasicrystal in a three-dimensional parameter space consisting of the shoulder width, temperature and density.

In the last part of this study, we make use of the following three interaction potentials, which exhibit two characteristic length scales:

- Hard-core linear ramp (HCLR) potential, which is written as

$$V_{\text{HCLR}}(r) = \begin{cases} \infty, & r \leq \sigma \\ \epsilon \frac{\delta - r}{\delta - \sigma}, & \sigma < r \leq \delta \\ 0, & r > \delta \end{cases} \quad (2)$$

This model has previously been shown to demonstrate a density anomaly during cooling and also formed a decagonal quasicrystal [31]. In this study, we take the width of the ramp to be equal to that of the square shoulder in the HCSS model, i.e. $\delta = 1.40\sigma$.

- Hard-core modified exponential (HCME) potential represents a modified form of an exponential potential to fit inside the square shoulder. The pair potential $V_{\text{HCME}}(r)$ reads

$$V_{\text{HCME}}(r) = \begin{cases} \infty, & r \leq \sigma \\ \epsilon \exp\left[-\left(\frac{r - \sigma}{\lambda}\right)^m\right], & r > \sigma \end{cases} \quad (3)$$

The values of $m = 5$ and $\lambda = 0.31\sigma$ are used in this study.

- Hard-core Buckingham or exp-6 (HCE6) potential is a classical potential used to model the soft-interactions that describe the anomalous behaviour of atomic substances at high pressures resulting from core-softening [37, 38], and reads

$$V_{\text{HCE6}}(r) = \begin{cases} \infty, & r \leq \sigma \\ \frac{-6\epsilon}{\alpha - 6} \left[\exp\left(-\alpha \left(\frac{r}{\sigma} - 1\right)\right) - \alpha \left(\frac{\sigma}{r}\right)^6 \right], & r > \sigma \end{cases} \quad (4)$$

where the parameter α controls the steepness of the potential and is taken to be 15 in the present simulations.

In figure 2, we show a comparison between all four interaction potentials. The HCLR is a linear ramp along the diagonal between the core and the corona diameters. The HCME is a short-ranged exponential potential that fits within the square shoulder. It initially follows the shape of the square shoulder and then decreases exponentially. On the other hand, the HCE6 is a long-ranged exponential potential which initially follows the shape of the linear ramp and then extends beyond the square shoulder. The parameters of each potential are chosen such that the shape of the potential largely fits inside the square shoulder at $\delta = 1.40\sigma$.

We perform Monte Carlo (MC) simulations in the canonical (NVT) and isothermal-isobaric (NPT) ensembles. We

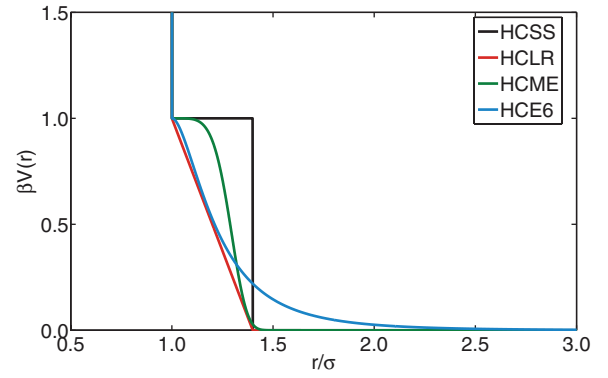


Figure 2. Comparison of the various two length scale interaction potentials used in this study shown as a function of the interparticle distance r . The pair potentials are the hard-core square shoulder (HCSS) potential, hard-core linear ramp (HCLR) potential, hard-core modified exponential (HCME) potential and the hard-core Buckingham or exp-6 (HCE6) potential.

use a rectangular box of area A with periodic boundary conditions. The hard-core diameter σ and the shoulder height ϵ are, respectively, taken to be the units of length and energy. We define the following dimensionless (reduced) quantities: temperature $T^* = k_B T / \epsilon$, pressure $P^* = \beta P \sigma^2$, and density $\rho^* = N \sigma^2 / A$, where $\beta = 1/k_B T$ is the inverse temperature with k_B the Boltzmann constant.

2.2. Structural analysis

We perform an array of analyses to study the local structure of the system and to differentiate between the phases. This comprises of constructing the polygonal tiling of the structure, calculating the m -fold bond orientational order parameter (BOO) of a particle j , χ_m^j , the average BOO of the system, χ_m , the m -fold bond orientational correlation function, $g_m(r)$, the radial distribution function, $g(r)$, and the static structure factor, $S(k)$. These parameters are explained below.

We obtain the polygonal tiling of a structure by drawing bonds between the neighbouring particles of each particle j , which are identified as particles that are at a centre-of-mass distance smaller than the square shoulder diameter δ from particle j . This is done to correlate the structures formed in our system with dodecagonal quasicrystals which are described in terms of tilings consisting of squares and equilateral triangles [39–43]. Analysis of the tiling allows us to distinguish between the various phases formed in the system and thus, the phase behaviour of the system. It is good to mention that such tilings have previously been used to study other phenomena in condensed matter systems like melting and condensation [44] and entropic demixing [45]. In our analysis of the tilings, we exclusively identify the triangle and the square tiles. We note that most of the defects in a hexagonal lattice result in a rhombic tile. Given the resemblance between the rhombus and square tiles, we also mark the rhombus tiles separately in order to prevent any effect of these tiles on the relative square-triangle tile calculations. Finally, the remainder of the tiles are grouped together and termed as ‘defect’ tiles. In the

Table 1. Method of classification of particle j according to its bond orientational order (BOO) χ_m^j .

Symmetry	BOO conditions	Colour scheme
Fluid/Other (OT)	$\chi_4^j, \chi_6^j, \chi_{12}^j < 0.5$	Orange
Crystal	$\chi_4^j, \chi_6^j, \chi_{12}^j > 0.5$	
- Square (SQ)	$\chi_4^j > \chi_6^j, \chi_{12}^j$	Purple
- Hexagonal (HX)	$\chi_6^j > \chi_4^j, \chi_{12}^j$	Green
- Dodecagonal (QC)	$\chi_{12}^j > \chi_4^j, \chi_6^j$	Red

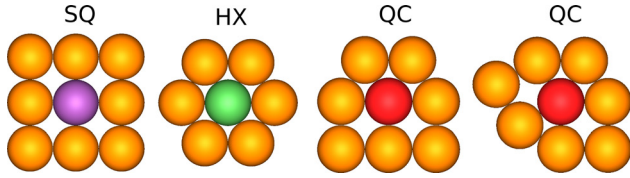


Figure 3. Colour scheme for classes of particles based on the BOO classification described in table 1.

tiling under study, we colour the triangles in green, squares in yellow, rhombi in orange and defects in grey.

The m -fold BOO of a particle j is defined as

$$\chi_m^j = \left| \frac{1}{N_B(j)} \sum_{k=1}^{N_B(j)} \exp(im\theta_{\mathbf{r}_{jk}}) \right|^2, \quad (5)$$

where m is the symmetry of interest, \mathbf{r}_{jk} is the centre-of-mass distance vector between two neighbours j and k , $\theta_{\mathbf{r}_{jk}}$ is the angle between \mathbf{r}_{jk} and an arbitrary axis, and $N_B(j)$ is the number of neighbours of particle j . For each particle j , we calculate χ_4^j representing square symmetry, χ_6^j representing hexagonal symmetry and χ_{12}^j representing dodecagonal symmetry. We use the method given in table 1 to classify particles based on their BOO. We consider a particle to be fluid-like if each of the three χ_m^j is less than 0.5. On the other hand, if each of χ_m^j is greater than 0.5, then a particle is said to have symmetry $m1$ if χ_{m1}^j is greater than the other two, namely χ_{m2}^j and χ_{m3}^j . Further, we identify and colour particles according to the following scheme: particles of square symmetry in purple, those of hexagonal in green, dodecagonal in red and fluid-like in orange as shown in figure 3.

The average BOO of the system is then written as [46]

$$\chi_m = \frac{1}{N} \sum_{j=1}^N \chi_m^j. \quad (6)$$

Ultimately, the m -fold bond orientation correlation function $g_m(r)$ with $r = |\mathbf{r} - \mathbf{r}'|$ is calculated as

$$g_m(r) = \left\langle \chi_m^j(\mathbf{r}) \cdot \chi_m^{k*}(\mathbf{r}') \right\rangle. \quad (7)$$

The radial distribution function $g(r)$ of a system calculated at a density ρ gives the probability of finding a pair of particles at a distance $r = |\mathbf{r} - \mathbf{r}'|$, and reads as

$$g(r) = \frac{1}{\rho^2} \left\langle \sum_{j=1}^N \sum_{k \neq j}^N \delta(\mathbf{r} - \mathbf{r}_j) \delta(\mathbf{r}' - \mathbf{r}_k) \right\rangle, \quad (8)$$

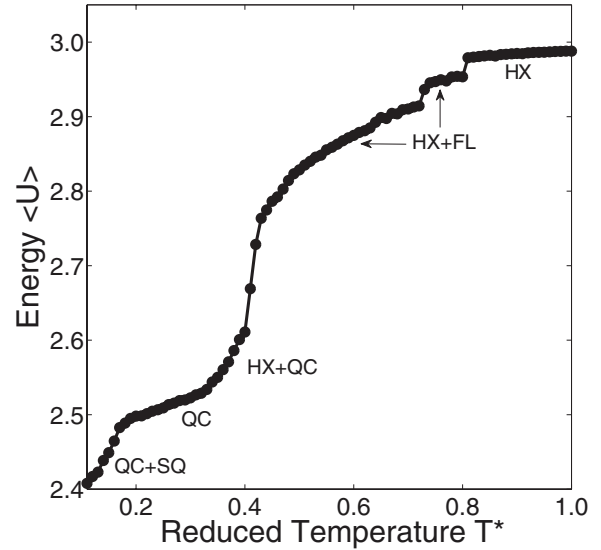


Figure 4. Potential energy per particle U as a function of (reduced) temperature ($T^* = k_B T / \epsilon$) for the HCSS system with shoulder width $\delta = 1.40\sigma$ at a constant (reduced) density $\rho^* = N\sigma^2/A = 0.98$. The phases marked are fluid (FL), hexagonal (HX), dodecagonal quasicrystal (QC) and square (SQ) phases.

where \mathbf{r}_j and \mathbf{r}_k are the positions of particles j and k , respectively. The static structure factor of the system is obtained by a Fourier transformation of the $g(r)$. It is represented in two-dimensional space as a diffraction pattern.

There are previous accounts of identifying quasicrystals using BOO, BOO correlation functions and radial distribution functions [29, 34]. In this work, we apprehend all these methods along with tiling calculations to provide a comprehensive overview of the various methods that can be used. We aim to verify the consistency achieved by using these methods in addition to studying the nature of quasicrystal formation.

3. Results and discussion

As indicated in the previous sections, this section will be presented in three parts. In the first part (section 3.1), we take a meticulous look at the process of formation of the dodecagonal quasicrystal in the HCSS system. In the second part (section 3.2), we study the influence of the shoulder width of the HCSS potential on the quasicrystal formation. And finally in the third part (section 3.3), we study the response of the system when the shape of the interaction potential is modified.

3.1. Formation of dodecagonal quasicrystal

By now, the presence of a random-tiling high-density dodecagonal quasicrystal in the HCSS system is well reported [29, 34, 36]. However, the process of its formation is seldom studied. It is formed either by cooling a hexagonal structure from a high to a low temperature at a constant density or by compressing an isotropic fluid phase to a higher density at a constant temperature. In this work, we delve into the former method where we cool a hexagonal lattice of (reduced) density $\rho^* = 0.98$ from (reduced) temperature $T^* = 1.0$ to 0.10.

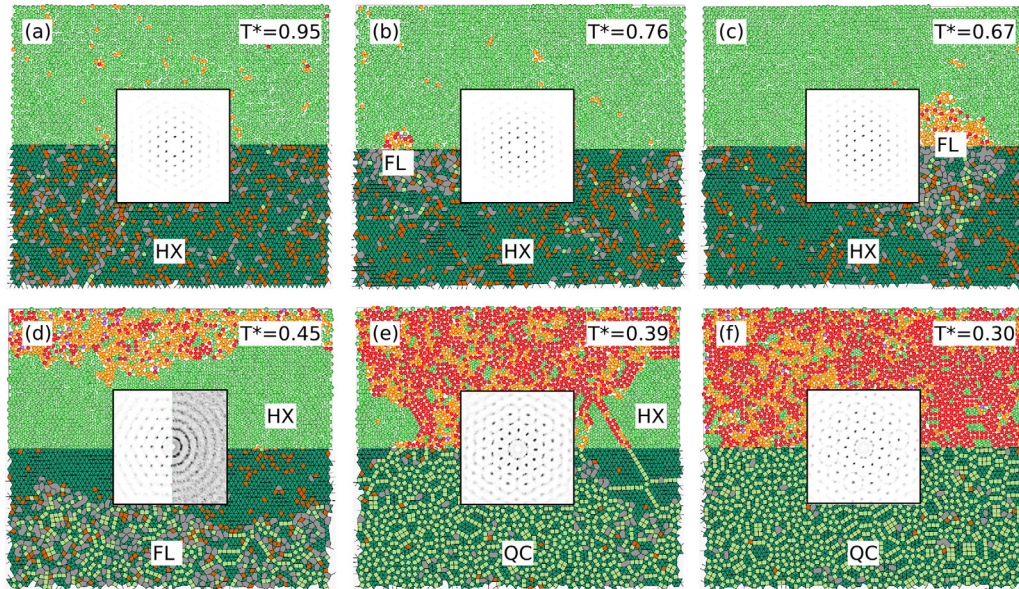


Figure 5. Phases formed at various temperatures ($T^* = k_B T/\epsilon$) during cooling of a hexagonal phase at a (reduced) density $\rho^* = N\sigma^2/A = 0.98$ interacting with a HCSS pair potential with a shoulder width $\delta = 1.40\sigma$. The phases marked are hexagonal (HX), fluid (FL) and dodecagonal quasicrystal (QC). Each panel consists of (top) positions of the hard cores of the particles, (bottom) polygonal tiling, (inset) calculated diffraction pattern of the structure. The particles and the tiles are, respectively, coloured according to the schemes explained in section 2.2.

To start, we inspect the change in the average potential energy of the system as a function of temperature. This is presented in figure 4. We note six different branches in the plot indicating distinct phase behaviors. We have marked these individual regions after studying various structural properties of the obtained configurations, for example, its tiling, BOO and corresponding diffraction patterns. In order to obtain a better understanding of these phase transformations, we study the energy plot in figure 4 in conjunction with typical configurations at a fixed temperature at each of these branches as shown in figure 5. These configurations as presented in figure 5 are composed of four features: (1) the positions of the hard cores of the particles are displayed at the top, (2) the polygonal tiling is presented at the bottom, (3) the calculated diffraction pattern is shown in the inset at the centre, and (4) the labels indicate the different phases. The colouring schemes used for the hard core of the particles in the top region and the tiles in the bottom region are explained in section 2.2.

Let us first take a qualitative look at the phase behaviour shown in figures 4 and 5 starting from high temperatures. At high temperature ($T^* > 0.80$), the potential energy decreases very slowly with decreasing temperature and is close to 3.0. The potential energy per particle of an ideal hexagonal lattice in the HCSS system with $\delta = 1.40\sigma$ is 3.0. Thus, the structure at these temperatures should be hexagonal in nature. However, the potential energy at these temperatures is not exactly equal to that of the perfect hexagonal lattice. This indicates the presence of defects, which are seen as the orange rhombi and other grey shapes in figure 5(a). Upon decreasing the temperature further, these individual defects accumulate and form a nucleus of the fluid phase as noticed in figure 5(b). A further decrease in temperature from $T^* = 0.72$ to 0.43 is characterised by a continuous decrease in potential energy. This refers

to the growth of the fluid nucleus (figure 5(c)). Towards the end of this growth regime, we observe a hexagonal–fluid phase coexistence (figure 5(d)). At $T^* = 0.45$ shown in figure 5(d), each of these phases occupy almost half of the simulation box and this allows us to calculate the diffraction pattern of the fluid and the hexagonal phase, separately. This is displayed in the inset of figure 5(d). When the temperature is decreased even further, we notice a sudden drop in the potential energy at $T^* \sim 0.41$. This drop coincides with the formation of a dodecagonal quasicrystal from the fluid, which results in the formation of a two-phase coexistence region between hexagonal and quasicrystal phases (figure 5(e)). It is affirmative to note that the diffraction pattern calculated at $T^* = 0.39$, shown in the inset of figure 5(e), clearly displays characteristics of both the quasicrystal and hexagonal structures. Comparing this transformation with the previous formation of the fluid from hexagonal, we note the absence of a single nucleus of the quasicrystal. However, the sudden change in the potential energy hints towards a first-order phase transition. With further lowering the temperature (and further decrease in energy), we observe a concurrent growth of the quasicrystal region and decline of the hexagonal region; the outcome of which is a dodecagonal quasicrystal spanning the entire simulation box (figure 5(f)). We remark that the energy in the quasicrystal regime is not constant, but decreases with decreasing temperature. This implies the formation of more squares at lower temperatures. Thus, the following energy drop is associated with the formation of a two-phase coexistence region between the square and quasicrystal phase.

Let us now quantitatively analyse the phase transformation with the help of order parameters as explained in section 2.2. In figures 6(a) and (b), we investigate the behaviour of the bond orientational order parameters. In figure 6(a), we plot

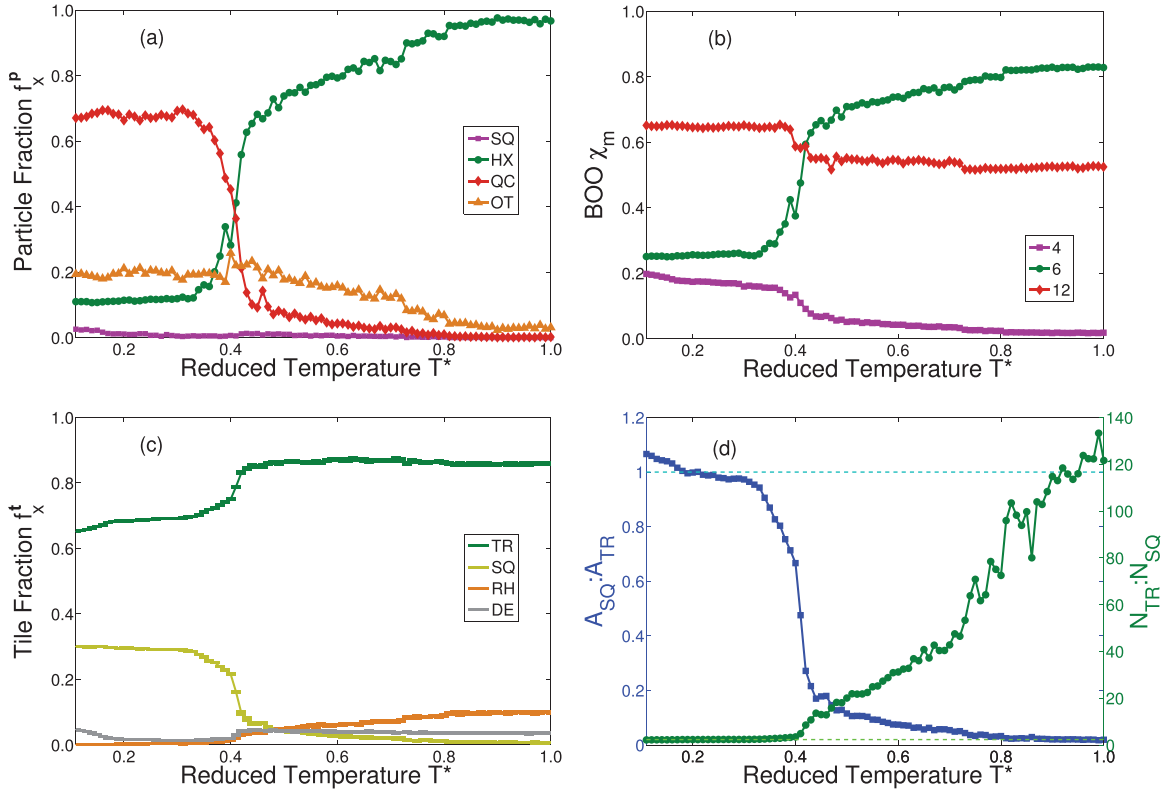


Figure 6. Various order parameters as a function of temperature ($T^* = k_B T / \epsilon$) describing the quasicrystal formation for the HCSS system with shoulder width $\delta = 1.40\sigma$ at a constant (reduced) density $\rho^* = N\sigma^2/A = 0.98$: (a) Fraction of different types of particles based on its BOO classification, f_X^p . The particle types X that we distinguish are square (SQ), hexagonal (HX), dodecagonal quasicrystal (QC), and others (OT). (b) m -fold bond orientational order (BOO) of the system, χ_m , with $m = 4, 6$, and 12 . (c) Fraction of different tile types, f_X^t . The tile types X that are considered are triangle (TR), square (SQ), rhombus (RH) and defects (DE). (d) Number and area ratio of square and triangle tiles. For convenience, the curves in (a)–(c) are coloured according to the same schemes as in figure 5.

the fraction of different types of particles as obtained from the BOO classification in table 1 as a function of temperature. The particle types X that we distinguish are square (SQ), hexagonal (HX), dodecagonal quasicrystal (QC), and others (OT). We notice that the fraction of hexagonal (f_{HX}^p) particles decrease and that of the quasicrystal (f_{QC}^p) particles increase with decreasing temperature indicating the formation of the quasicrystal from the hexagonal phase. However, the fraction of square particles (f_{SQ}^p) remains almost constant throughout the entire temperature range except at very low temperatures. This indicates that no square phase is formed during the initial quasicrystal formation, but there is a small indication of its formation at very low temperatures. Another interesting feature is the fraction of ‘fluid-like’ particles (f_{OT}^p). We observe a very low, but non-zero, value at high temperatures indicating defects in the hexagonal lattice. With decreasing temperature, we observe a significant increase in f_{OT}^p through the two-phase coexistence region of the hexagonal and fluid phase. This complies with the formation of larger amounts of fluid phase. This increase, however, ceases with the formation of the quasicrystal and the f_{OT}^p remains at a constant value. We further confirm the first-order nature of the fluid to the quasicrystal transformation from the sudden drop in f_{HX}^p and the simultaneous increase in f_{QC}^p .

Let us now pay attention to figure 6(b), where we plot the average m -fold bond orientational order as a function of temperature. On the one hand, we notice that the behaviour of χ_6 and χ_{12} , respectively, follow that of the fraction of hexagonal (f_{HX}^p) and quasicrystal (f_{QC}^p) particles in figure 6(a) i.e. χ_6 decreases and χ_{12} increases with decreasing temperature. However, on the other hand, unlike the constant behaviour of f_{SQ}^p , we find an increase in values of χ_4 at temperatures close to the quasicrystal formation. This further reinforces the fact that the formation of the quasicrystal is aided by the replacement of particles of hexagonal symmetry by ones with square symmetry. The increase in χ_4 values at even lower temperatures $T^* \sim 0.18$ indicates the formation of the square phase.

Next, we correlate the behaviour of the particles with that of the tilings obtained from connecting the nearest neighbours of particles. To do so, we plot the behaviour of the fraction of tiles during cooling of the system in figures 6(c) and (d). Figure 6(c) shows the fraction of triangle tiles f_{TR}^t , square tiles f_{SQ}^t , rhombus tiles f_{RH}^t , and defect tiles f_{DE}^t as a function of temperature. The fraction of triangle tiles f_{TR}^t is almost constant in the temperature range where the hexagonal phase and fluid-hexagonal phase coexistence are observed. The difference between these two regions is brought about by the relative fractions of the rhombus tiles f_{RH}^t and defect tiles

f_{DE}^t . In the temperature range where the hexagonal phase is found, we observe a larger fraction of rhombus tiles f_{RH}^t representing the defects in the hexagonal lattice. Upon lowering the temperature, we find an increase in the fraction of defect tiles f_{DE}^t signalling the formation of the fluid phase. At lower temperatures, closer to the quasicrystal formation, we observe a simultaneous decrease in the fraction of rhombus tiles f_{RH}^t and defect tiles f_{DE}^t and an increase in the fraction of square tiles f_{SQ}^t . We note the almost constant values of f_{TR}^t and f_{SQ}^t in the quasicrystal region. In the low temperature regime of the quasicrystal region, we note a further increase in f_{SQ}^t denoting the formation of the square phase. These observations are concurrent with those of the particle fractions in figure 6(a).

Now, we turn our attention to figure 6(d), where we study the composition of the tiling in terms of the constituent square and triangle tiles. This is done because the dodecagonal quasicrystals described by a square-triangle tiling have a triangle-to-square number ratio of $4/\sqrt{3} \simeq 2.309$ [43]. At this ratio, both the square and triangle occupy equal areas, thereby giving a triangle-to-square area ratio of 1. Thus, in figure 6(d), we show the ratio of (1) the areas of square and triangle tiles, and (2) the number of triangles and squares as a function of temperature. We have also marked the ideal triangle-to-square area and number ratios using dashed lines. The prominent observation that results from this plot is that both the area and the number ratios are close to their ideal values in the range of temperatures pertaining to the quasicrystal region. Furthermore, the increase in the area ratio towards the end of the temperature spectrum coincides with the formation of the SQ phase.

Finally, we examine the long-range orientational order of the system by means of the radial distribution function $g(r)$ and the 6- and 12- fold bond orientational correlation functions $g_6(r)$ and $g_{12}(r)$. These quantities are shown in figure 7 as a function of temperature. The curves corresponding to different phases are separately marked. In figure 7(a), we see the evolution of the $g(r)$ from the hexagonal (HX) to the quasicrystal (QC) phase upon decreasing the temperature. The initial peaks of the $g(r)$ of the HX phase lies at 1.0σ and $\sqrt{3} \sim 1.732\sigma$ denoting the hard-core diameter and a sequence of consecutive equilateral triangles, respectively. The formation of quasicrystals is indicated by the appearance of a peak at 1.4σ (marked by an arrow in figure 7(a)) corresponding to a sequence of squares. In figure 7(b), we present the 6-fold and 12-fold bond orientational correlation functions $g_6(r)$ and $g_{12}(r)$, respectively. Both the $g_6(r)$ and $g_{12}(r)$ reach a constant value for the hexagonal and quasicrystal phases and do not decline to zero at larger r . This confirms the presence of long-range orientational order in the system. As can be expected, the $g_6(r)$ of the HX phase is higher than that of the QC phase; while the inverse holds for $g_{12}(r)$. This confirms the dominant orientational order in these phases. Also, the decaying nature of both the $g_6(r)$ and $g_{12}(r)$ curves at temperatures $T^* = 0.4$ and 0.5 indicates the absence of long-range orientational order in the system, i.e. the presence of a fluid (FL) phase. The value of $g_{12}(r)$ decreases from $T^* = 0.30$ to 0.10 indicating the ‘loss’ of fraction of QC phase,

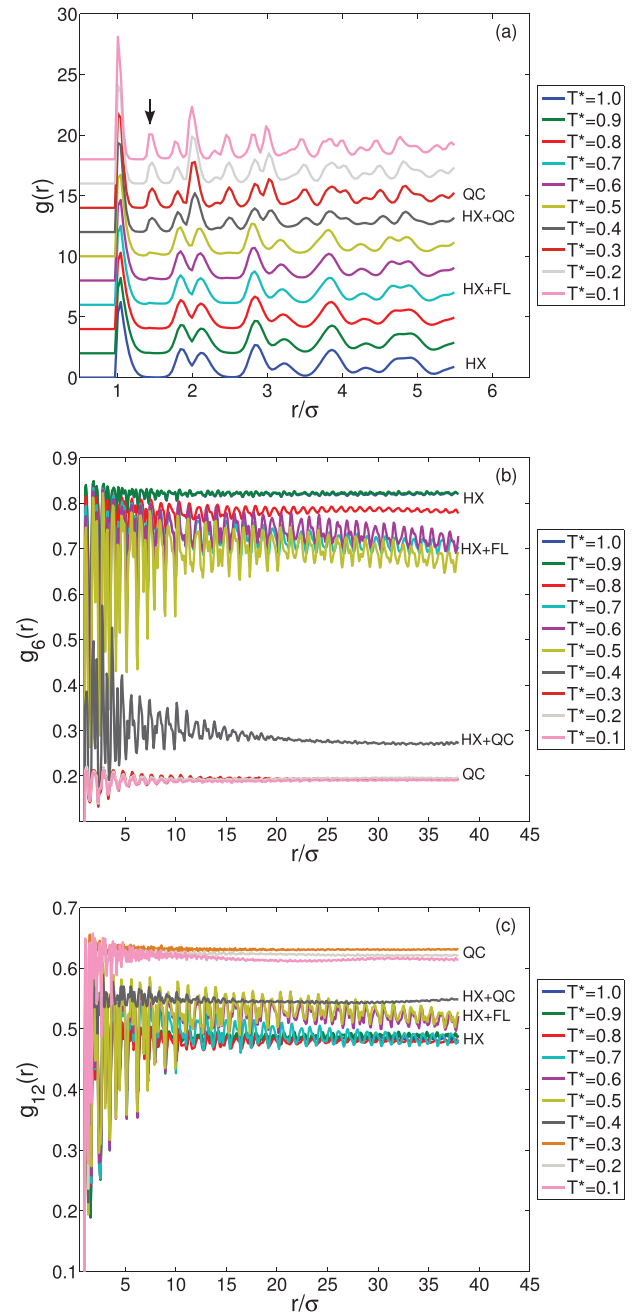


Figure 7. Structural properties as a function of temperature during quasicrystal formation: (a) radial distribution function $g(r)$, (b) 6-fold bond orientation correlation function $g_6(r)$, and (c) 12-fold bond orientation correlation function $g_{12}(r)$. The phases indicated are hexagonal (HX), fluid (FL), dodecagonal quasicrystal (QC). For clarity, we shifted the $g(r)$ in (a) in the vertical direction by $\Delta y = 2$.

i.e. the formation of another phase in the system. From our previous discussions, we know this to be the square (SQ) phase.

To summarise this section, we have investigated the formation of the QC phase by cooling a hexagonal phase at a constant density. Upon lowering the temperature, we first find the formation of a fluid phase via a nucleation and growth mechanism, resulting into a phase coexistence of the fluid and hexagonal phase. By further cooling the system, we find that a QC phase forms within the fluid phase, and continues to grow until the whole system is quasicrystalline.

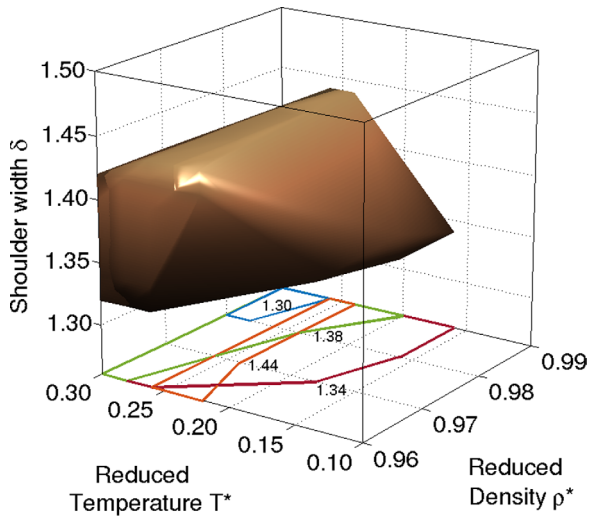


Figure 8. Three-dimensional phase space of (reduced) density ρ^* , temperature T^* and shoulder width δ where the dodecagonal quasicrystal (QC) is observed as denoted by the coloured volume for the HCSS system. The reduced quantities are defined as $T^* = k_B T / \epsilon$ and $\rho^* = N \sigma^2 / A$. The box represents the range of data points that were considered. The contours in the $\rho^* - T^*$ plane for a few shoulder widths are also given.

3.2. Effect of shoulder width

The calculations discussed in the above section were performed at a single value of the width of the square shoulder. Here, we assess the effect of the shoulder width on the formation of the dodecagonal quasicrystal by performing simulations in the NVT ensemble at shoulder widths δ from 1.26σ to 1.50σ , densities ρ^* between 0.96 and 0.99, and temperatures T^* between 0.10 and 0.30. We analyse the resulting configurations with the help of their polygonal tiling, diffraction pattern and average bond orientational order (BOO) of the system, χ_m .

We observe the formation of the dodecagonal quasicrystal (QC) in a range of densities, temperatures and shoulder widths. This three-dimensional phase space is given in figure 8. The coloured volume shown represents the limits of the quasicrystal formation and the box displays the range of data points simulated. We also plot the contours in the density-temperature plane for a few shoulder widths. It is evident from these plots that the quasicrystal forms over a range of all three parameters. For clarity, we perform further analysis at constant temperature $T^* = 0.28$.

We plot the state diagram in the shoulder width-density ($\delta - \rho^*$) plane at $T^* = 0.28$ in figure 9. At shoulder widths $\delta \geq 1.46\sigma$, we find that the system behaves similar to the hard-disk model. Even though we only observe a HX + FL phase coexistence at the densities shown here, it is apparent that this region will be bordered by FL at lower densities and HX at higher densities. Further, we recognise the formation of the dodecagonal quasicrystal QC over a range of shoulder widths $1.30\sigma \leq \delta \leq 1.44\sigma$. Lastly, we note that at even lower shoulder widths $\delta \leq 1.30\sigma$, we find a 18-fold symmetric quasicrystal (QC18), which was previously reported by Dotera *et al* at $\delta = 1.27\sigma$.

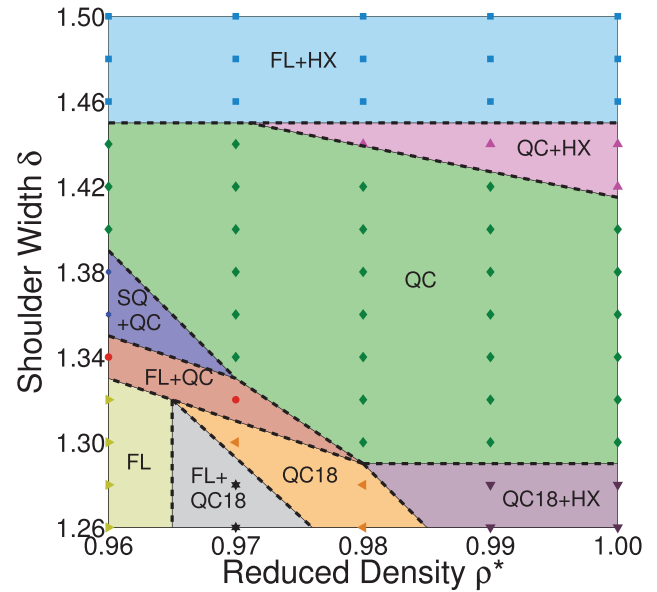


Figure 9. State diagram in the shoulder width δ -reduced density ρ^* plane for the two-dimensional HCSS system at (reduced) temperature $T^* = 0.28$. All quantities are represented in reduced units as $T^* = k_B T / \epsilon$ and $\rho^* = N \sigma^2 / A$. The phases represented are fluid (FL), hexagon (HX), square (SQ), dodecagonal quasicrystal (QC) and octadecagonal quasicrystal (QC18).

This state diagram is substantiated by the calculation of 4-, 6-, 12-, and 18- fold BOO at each condition of density and shoulder width. This is plotted as four separate surface plots in figure 10. In the χ_4 plot given in figure 10(a), we notice higher values of the order parameter at lower densities and moderate shoulder widths indicating the presence of the SQ phase. Looking at figure 10(b), we confirm higher χ_6 values at higher densities and shoulder widths showing the presence of the HX phase. It is interesting to note that at these conditions of densities and shoulder widths where the HX phase is found, the values of χ_6 , along with χ_{12} and χ_{18} shown respectively in figures 10(c) and (d) are in the order $\chi_6 > \chi_{12} > \chi_{18}$. This is because the χ_{12} and χ_{18} are respectively the 2nd and 3rd order terms of χ_6 . Thus, when χ_6 is non-zero, the χ_{12} and χ_{18} parameters will also have a non-zero value which decreases with increasing order of symmetry. Lastly, the dominant phase in the lower right quadrant is recognised to be the QC18; while the dodecagonal quasicrystal QC is formed at all densities in the middle range of the shoulder widths considered. In summary, we recognise that the calculations shown here validates the state diagram in figure 9 and shows that the QC is formed over a range of shoulder widths, temperatures and densities.

3.3. Effect of shape of interaction potential

The HCSS system is a minimalistic approach to model the core-corona architecture of colloidal particles. However, the assumption of a constant repulsion through the entire width of the shoulder is not experimentally realisable owing to the non-uniformity in the shape and size of the polymer brushes that surround the solid core. Thus, to account for this non-uniformity, we examine the effect of shape of the interaction

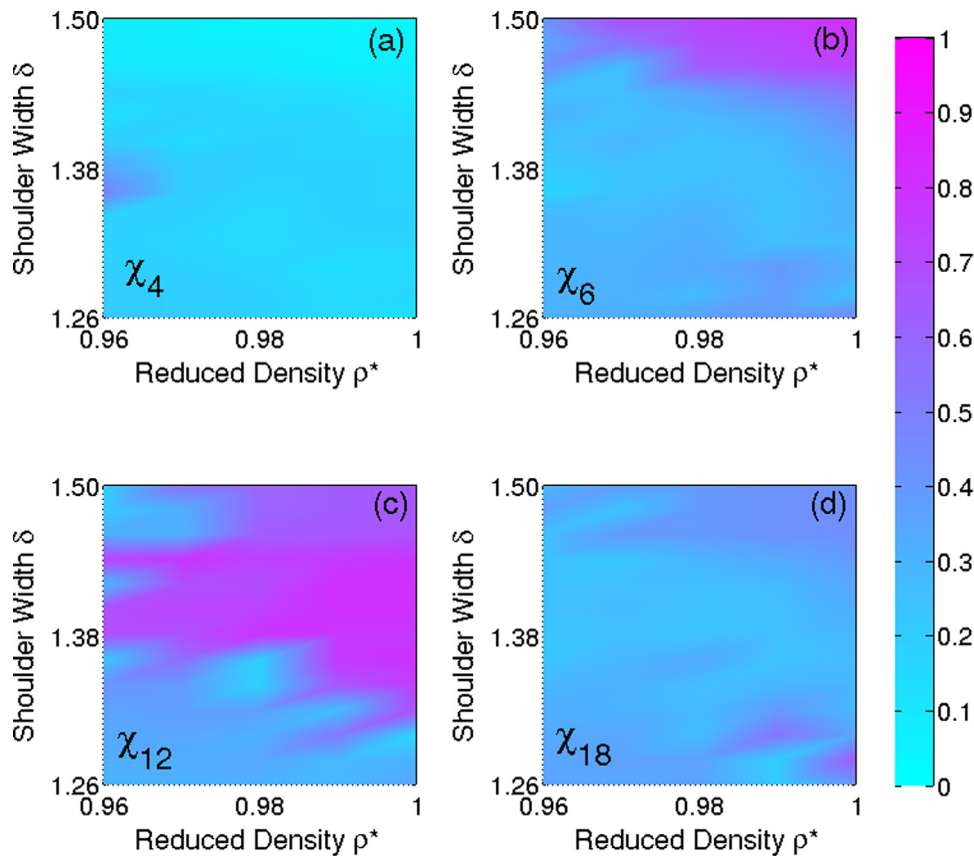


Figure 10. Average bond orientational order parameters representing square χ_4 , hexagonal χ_6 , dodecagonal χ_{12} and octadecagonal χ_{18} symmetries as a function of density $\rho^* = N\sigma^2/A$ and shoulder width δ at (reduced) temperature $T^* = k_B T/\epsilon = 0.28$.

potential without effectively altering the characteristic length scales in this work. In other words, we modify the shape of the interaction potential while keeping the core size, the corona size, and the repulsive strength at the core intact.

We wish to point out to the readers that a similar study was recently reported by Schoberth *et al* [34] wherein they accounted for an increasing repulsive force in the corona mimicking the entropic interactions of spherical polymer brushes in core-shell micelles. Their assumption, in turn, results in (1) smoothening of both characteristic length scales, viz. the core and corona diameter, and (2) increased repulsive forces near the core. In our present study, we maintain the bounds of the two length scales and the maximum interaction strength near the core at the same values as the HCSS system; i.e. we only modify the shape of the curve in the corona region.

For this study, we make use of three other potentials in addition to the hard-core square-shoulder (HCSS) potential; namely hard-core linear-ramp (HCLR) potential, hard-core modified-exponential (HCME) potential, and hard-core Buckingham or exp-6 (HCE6) potential. The details regarding these potentials are given in section 2. We compare the phases formed in systems with each of these potentials at a range of densities and temperatures. For the HCSS and HCLR potentials, we calculate the respective equilibrium phase diagrams using free-energy calculations; while for the other two potentials namely HCME and HCE6, we plot the state diagrams resulting from simulations in the NVT ensemble at each density and temperature. The process of mapping out the phase

diagram for the HCSS system is explained in our previous publication [36] and we follow a similar procedure for the HCLR system. In the aforementioned publication, we also present an account of the HCSS phase diagram. For comparison purposes, the HCSS phase diagram is replotted here.

The calculated phase diagrams and state diagrams are given in figure 11. The potential corresponding to each of these plots along with the outlining square shoulder is shown in the respective insets. In general, we report that the same phases are formed in all these systems. The phases comprise of fluid (FL), square (SQ), low- and high-density hexagonal (LDH, HDH) and dodecagonal quasicrystal (QC). The formation of the hexagonal phase in two density ranges is driven by the presence of two-length scales in the interaction potentials such that the interparticle distances in LDH and HDH are at the core and corona diameters, respectively. We make the following observations regarding the QC phase. First, we find that the QC phase is found in all four cases; and second, the temperature of formation of the QC depends on the interaction potential. The first observation regarding the QC phase in all these systems affirms that the presence of two length scales in the interaction potential is a prerequisite for the formation of a quasicrystal in single component colloidal systems. The shape of the interaction potential inside the corona does not matter for the QC formation as long as the two length scales are uniquely defined. The second observation is related to the temperature range where the QC is formed. We find that the temperature range shifts to lower temperatures

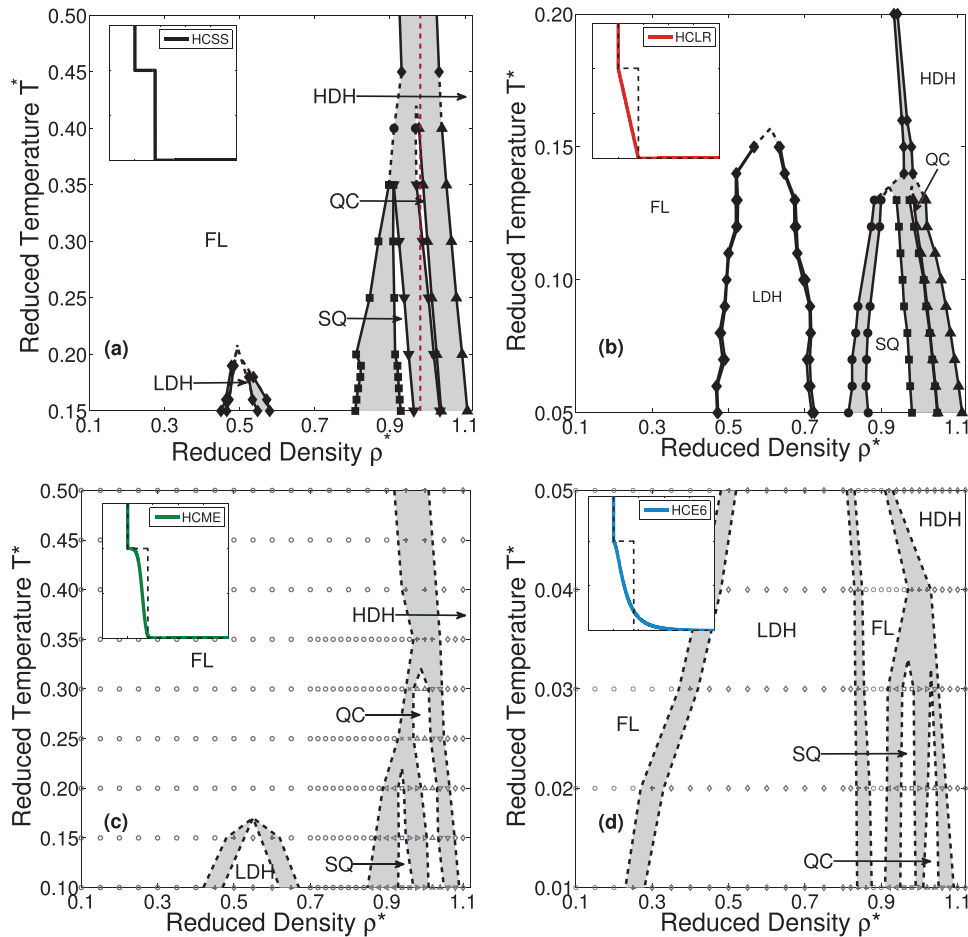


Figure 11. Effect of interaction potential on quasicrystal formation: phase diagram ((a) and (b)) and state diagram ((c) and (d)) in the (reduced) temperature-density plane obtained for systems interacting with (a) hard-core square shoulder potential (HCSS) taken from [36] (b) hard-core linear ramp potential (HCLR) (c) hard-core modified exponential potential (HCME) (d) hard-core exp-6 potential (HCE6). Please note that the temperature axis in the figures are different. The reduced units are $T^* = k_B T / \epsilon$ and $\rho^* = N \sigma^2 / A$. The phases shown are fluid (FL), low-density hexagonal (LDH), square (SQ), dodecagonal quasicrystal (QC) and high-density hexagonal (HDH). The lines act as guides to the eye, and the open symbols in (c) and (d) denote the state points that were considered in the simulations. The red dashed line in (a) follows the cooling simulation performed in section 3.1.

when the interparticle potential becomes less repulsive going from the HCSS to the HCME and the HCLR potential, i.e. the energy penalty for the particles to be in the middle of the corona decreases. Thus, a higher interaction strength (or lower temperature) is required to compensate for this penalty loss. This interaction strength can be tuned by varying the density of polymer brushes in experimental core-corona systems. Supplementary to this energy penalty loss, one also needs to account for the much larger corona size ($\sim 2.5\sigma$) in the HCE6 system. This large corona size is a result of the long exponential tail in the potential. This results in a much lower temperature for the formation of the QC in the HCE6 system in comparison to the other three.

In summary, we find that the dodecagonal quasicrystal is formed irrespective of the shape of the interaction potential, as long as the two length scales are maintained. The shape of the potential does affect the temperature range in which the dodecagonal quasicrystal is stable.

4. Conclusions

We investigated the formation of a colloidal dodecagonal quasicrystal in a simple model of particles interacting with a potential consisting of a hard core of diameter σ and a repulsive square shoulder of diameter $\delta = 1.40\sigma$. We scrutinised the formation process using bond order parameters, correlation functions and tiling fractions in the first part of this work. Upon cooling the hexagonal phase at a constant density, we find the nucleation and growth of a fluid phase, resulting in a two-phase coexistence of the fluid and hexagonal phase. Lowering the temperature further, we find that the quasicrystal forms from the fluid phase. Finally, it is worth noting that the different phase transformations encountered during the cooling process is consistent with the phase diagram as presented in figure 11.

In the second part of this work, we studied the formation of the dodecagonal quasicrystal for a range of shoulder widths,

temperatures and densities. We found that the quasicrystal formation is robust with respect to all three parameters. For example, at a temperature $T^* = 0.28$, we find that the quasicrystal is formed at densities ρ^* between 0.96 and 1.00 and shoulder widths δ between 1.30σ and 1.44σ .

In the last part we studied the effect of the shape of the interaction potential on the formation of the quasicrystal. We used four interaction potentials each of which have two inherent length scales, namely a hard-core potential supplemented with a square shoulder, a linear ramp, a modified exponential, or a Buckingham (exp-6) potential. We observed the formation of a dodecagonal quasicrystal in all these systems. However, the shape of the potential influences the temperature range of the stability regime of the quasicrystal formation.

Our studies provide a comprehensive summary of parameters that can be used to identify quasicrystals in soft matter systems including bond order parameters, bond correlation functions and tiling calculations. Furthermore, our investigations provide insight to the robustness of the formation of the quasicrystal, which is of considerable importance for performing experimental studies on these systems. This could enable tailoring of experiments to synthesise more quasicrystal-forming systems.

Acknowledgments

This work is part of the Industrial Partnership Programme ‘Computational Sciences for Energy Research’ (12CSER004) of the Foundation for Fundamental Research on Matter (FOM), which is part of the Netherlands Organisation for Scientific Research (NWO). This research programme is co-financed by Shell Global Solutions International BV We thank Wessel S Vlug for performing the calculations to identify polygonal tiles and Simone Dussi for critical reading of the manuscript.

References

- [1] Shechtman D and Blech I 1984 *Phys. Rev. Lett.* **53** 1951
- [2] Zeng X, Ungar G, Liu Y, Percec V, Dulcey A E and Hobbs J K 2004 *Nature* **428** 157
- [3] Fischer S and Exner A 2011 *Proc. Natl. Acad. Sci.* **108** 1810–4
- [4] Takano A, Kawashima W, Noro A, Isono Y, Tanaka N, Dotera T and Matsushita Y 2005 *J. Polym. Sci. B* **43** 2427
- [5] Dotera T and Gemma T 2006 *Phil. Mag.* **86** 1085
- [6] Hayashida K, Dotera T, Takano A and Matsushita Y 2007 *Phys. Rev. Lett.* **98** 195502
- [7] Lee S, Bluemle M J and Bates F S 2010 *Science* **330** 349
- [8] Talapin D V, Shevchenko E V, Bodnarchuk M I, Ye X, Chen J and Murray C B 2009 *Nature* **461** 964
- [9] Bodnarchuk M I, Erni R, Krumeich F and Kovalenko M V 2013 *Nano Lett.* **13** 1699–705
- [10] Roichman Y and Grier D 2005 *Opt. Express* **13** 5434
- [11] Mikhael J, Roth J, Helden L and Bechinger C 2008 *Nature* **454** 501
- [12] Steurer W and Sutter-Widmer D 2007 *J. Phys.: D. Appl. Phys.* **40** R229
- [13] Maciá E 2012 *Rep. Prog. Phys.* **75** 036502
- [14] Vardeny Z, Nahata A and Agrawal A 2013 *Nat. Photon.* **7** 177–87
- [15] Busch K and John S 1998 *Phys. Rev. E* **58** 3896
- [16] Krauss T F and De La Rue R M 1999 *Prog. Quantum Electron.* **23** 51
- [17] Xia B Y, Byron G, Yadong Y and Yu L 2000 *Adv. Mater.* **12** 693
- [18] Zoorob M, Charlton M, Parker G, Baumberg J and Netti M 2000 *Nature* **404** 740
- [19] Lifshitz R and Petrich D 1997 *Phys. Rev. Lett.* **79** 1261
- [20] Rucklidge A M and Silber M 2007 *Phys. Rev. E* **75** 1
- [21] Dotera T 2011 *Isr. J. Chem.* **51** 1197
- [22] Barkan K, Diamant H and Lifshitz R 2011 *Phys. Rev. B* **83** 172201
- [23] Archer A J, Rucklidge A M and Knobloch E 2013 *Phys. Rev. Lett.* **111** 165501
- [24] Archer A J, Rucklidge A M and Knobloch E 2015 *Phys. Rev. E* **92** 012324
- [25] Leung P W, Henley C L and Chester G V 1989 *Phys. Rev. B* **39** 446
- [26] Strandburg K J 1989 *Phys. Rev. B* **40** 6071
- [27] Salgado-blanco D and Mendoza C I 2015 *Soft Matter* **11** 889
- [28] Engel M and Trebin H R 2007 *Phys. Rev. Lett.* **98** 225505
- [29] Dotera T, Oshiro T and Zihel P 2014 *Nature* **506** 208
- [30] Skibinsky A, Buldyrev S V, Scala A, Havlin S and Stanley H E 1999 *Phys. Rev. E* **60** 2664
- [31] Jagla E A 1998 *Phys. Rev. E* **58** 1478
- [32] Costa Campos L Q, de Souza Silva C C and Apolinario S W S 2012 *Phys. Rev. E* **86** 051402
- [33] Engel M, Damasceno P F, Phillips C L and Glotzer S C 2014 *Nat. Mater.* **14** 109
- [34] Schoberth H G, Emmerich H, Holzinger M, Dulle M, Förster S and Gruhn T 2016 *Soft Matter* **12** 7644
- [35] Young A D and Alder B J 1977 *Phys. Rev. Lett.* **38** 1213
- [36] Pattabhiraman H, Gantapara A P and Dijkstra M 2015 *J. Chem. Phys.* **143** 164905
- [37] Malescio G, Saija F and Prestipino S 2008 *J. Chem. Phys.* **129** 127
- [38] Buldyrev S V, Malescio G, Angell C A, Giovambattista N, Prestipino S, Saija F, Stanley H E and Xu L 2009 *J. Phys.: Condens. Matter* **21** 504106
- [39] Li W, Park H and Widom M 1992 *J. Stat. Phys.* **66** 1
- [40] Baake M, Klitzing R and Schlottmann M 1992 *Physica A* **191** 554
- [41] Widom M 1993 *Phys. Rev. Lett.* **70** 2094
- [42] Nienhuis B 1998 *Phys. Rep.* **301** 271
- [43] Ishimasa T 2011 *Isr. J. Chem.* **51** 1216
- [44] Kawamura H 1980 *Prog. Theor. Phys.* **63** 24–41
- [45] Wojciechowski K W 1996 *Physica A* **232** 723
- [46] Weber H, Marx D and Binder K 1995 *Phys. Rev. B* **51** 14636